Physics of Fluids

Relations between Reynolds stresses and their dissipation rates during premixed flame–wall interaction within turbulent boundary layers

Umair Ahmed ✉ (ID) ; Sanjeev Kumar Ghai (ID) ; Nilanjan Chakraborty (ID)

Check for updates

View Online

Export Citation

19 April 2024 12:11:51

Physics of Fluids

Special Topic:

Flow and Lipid Nanoparticles

Guest Editors: Richard Braatz and Mona Kanso

Submit Today!

AIP Publishing

AIP Publishing
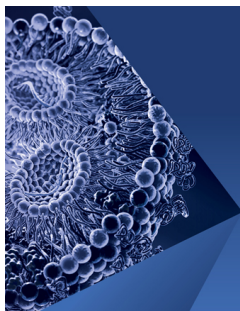
Relations between Reynolds stresses and their dissipation rates during premixed flame–wall interaction within turbulent boundary layers

View Online   Export Citation   CrossMark

Umair Ahmed,[a]) 🔬 Sanjeev Kumar Ghai, 🔬 and Nilanjan Chakraborty 🔬

AFFILIATIONS

School of Engineering, Newcastle University, Newcastle upon Tyne NE1 7RU, United Kingdom

[a])Author to whom correspondence should be addressed: umair.ahmed@newcastle.ac.uk

ABSTRACT

A direct numerical simulation (DNS) database for head-on quenching of premixed flames propagating across turbulent boundary layers representative of friction Reynolds numbers, Re_τ, of 110 and 180 has been utilized to analyze the interrelation between Reynolds stresses and their dissipation rates during flame–wall interaction. The Reynolds stresses and their dissipation rates exhibit significant deviations from the corresponding non-reacting flow profiles within the flame brush and in the burned gas region. This behavior is prominent for the components in the wall-normal direction because the mean direction of flame normal acceleration due to thermal expansion aligns with the wall-normal direction in this configuration. The anisotropy of Reynolds stresses and their dissipation rate tensors have been found to be qualitatively similar, but the anisotropic behavior weakens with increasing Re_τ. However, the components of the anisotropy tensors of Reynolds stresses and viscous dissipation rate are not related according to a linear scaling, and thus, the models based on this assumption do not successfully capture the viscous dissipation rate components obtained from the DNS data. By contrast, a model, which includes the invariants of the anisotropy tensor of Reynolds stresses and satisfies the limiting conditions, has been found to capture especially the diagonal components of the viscous dissipation rate tensor more successfully for both non-reacting and reacting cases considered in this work. However, the quantitative prediction of this model suffers for the components in the wall-normal direction for lower values of Re_τ, but the performance of this model improves with an increase in Re_τ.

I. INTRODUCTION

The closure of Reynolds stresses motivates the need for turbulence modeling in the context of Reynolds averaged Navier–Stokes (RANS) simulations. The Reynolds stress is defined as $\widetilde{u_i'' u_j''}$, where u_i is the ith component of velocity and $\overline{q}$, $\widetilde{q} = \overline{\rho q}/\overline{\rho}$, and $q'' = q - \widetilde{q}$ refer to the Reynolds average, Favre-average, and Favre fluctuation of a general variable q, respectively, with ρ being the gas density. The effects of heat release induce additional effects on Reynolds stresses in turbulent premixed combustion,[1–4] which make the closure of Reynolds stresses for turbulent reacting flows more challenging than non-reacting flows. The statistical behavior and modeling of viscous dissipation rate tensor[3,5] [i.e., $\widetilde{\varepsilon_{ij}} = 2\overline{\mu(\partial u_i''/\partial x_k)(\partial u_j''/\partial x_k)}/\overline{\rho}$] play key roles in the closure of the Reynolds stress transport equation in non-reacting flows, and these aspects are particularly important for the modeling of wall-bounded flows. It has been demonstrated in previous analyses[1–4] that the flame normal acceleration induced by thermal

expansion can have a significant influence on the statistical behavior and modeling of the Reynolds stress tensor in turbulent premixed flames. The statistical behavior and modeling of the viscous dissipation rate of the Reynolds stress tensor are rarely analyzed for turbulent premixed flames.[6] Moreover, all the existing analyses[2–4] in premixed combustion, which dealt with the viscous dissipation rate, were carried out for flows without any influence of walls. The heat release rate due to combustion and local quenching of flame caused by the heat loss through the wall within the turbulent boundary layer can potentially affect the anisotropy of both Reynolds stress tensor and its dissipation rate.[2–4]

The anisotropy of Reynolds stresses plays a key role in the modeling of the pressure strain term in the Reynolds stress transport equation[7] (e.g., return to isotropy approaches), and this is also important in the premixed combustion modeling using second moment closure.[8–12] The second-moment closure, where the Reynolds stress transport is solved, has been found to provide better predictions of turbulence

19 April 2024 12:11:51

quantities than eddy viscosity models in complex flow configurations[13–15] for which large eddy simulation (LES) turns out to be too expensive in comparison to RANS. A large extent of uncertainty is associated with the modeling of $\widetilde{\varepsilon}_{ij}$,[11,16] and thus, an improved approach for dissipation rate modeling is necessary. Thus, the understanding of anisotropy of Reynolds stress and its dissipation rate tensor along with its modeling are likely to yield improved predictions of turbulent kinetic energy and its dissipation rate in the context of second-moment closure.[11] It is important to note that turbulent kinetic energy, $\widetilde{k}$, and its dissipation rate, $\widetilde{\varepsilon}$, are often used as input parameters for combustion models (e.g., flame surface density[17] and scalar dissipation rate[18] based closures), and thus, their accurate predictions will in turn improve the predictive capabilities of combustion models in RANS simulations of premixed flames.

The statistical behaviors of $\widetilde{u_i'' u_j''}$ and $\widetilde{\varepsilon}_{ij}$ tensors are rarely analyzed for premixed flame–wall interaction (FWI) within turbulent boundary layers[19] although this information is vital for the Reynolds stress, $\widetilde{u_i'' u_j''}$, transport in the case of hybrid RANS/LES modeling strategies for wall-bounded turbulent reacting flows. It should be recognized here that the linear eddy viscosity based models relying on the conventional Boussinesq's hypothesis are often rendered invalid in premixed flames.[20–23] Thus, for the purpose of hybrid RANS/LES of turbulent premixed FWI, it might be useful to consider Reynolds stress closures instead of models employing the Boussinesq's hypothesis. Furthermore, in complex engineering configurations, the near wall secondary flow features are better represented by the second moment closure type models when compared with the one or two equation linear eddy viscosity based models.[13,14,24] Hence, it may be useful to consider the second moment closure in the context of hybrid RANS/LES of turbulent reacting flows at least in some configurations. In order to understand the interrelation between $\widetilde{u_i'' u_j''}$ and $\widetilde{\varepsilon}_{ij}$, the current analysis focuses on the statistical behaviors of $\widetilde{u_i'' u_j''}$ and $\widetilde{\varepsilon}_{ij}$ tensors using direct numerical simulations (DNS) for head-on quenching (HOQ) of statistically planar flames propagating toward inert isothermal walls across turbulent boundary layers representative of friction Reynolds numbers, Re_τ, of 110 and 180.

In this respect, the main objectives of this analysis are (a) to compare the variations of $\widetilde{u_i'' u_j''}$ and $\widetilde{\varepsilon}_{ij}$ at different stages of FWI with the corresponding statistics for non-reacting fully developed channel flows along with physical explanations for the observed behavior, (b) to analyze the interrelation between $\widetilde{u_i'' u_j''}$ and $\widetilde{\varepsilon}_{ij}$ during head-on quenching of premixed flames within turbulent boundary layers and its implications on the modeling of $\widetilde{\varepsilon}_{ij}$, and (c) to demonstrate the effects of Re_τ on the statistics related to (a) and (b). The remainder of the paper is organized in the following manner. The mathematical background and numerical implementation of the DNS database are described in Secs. II and III, respectively. This is followed by the presentation and discussion of results in Sec. IV. The main findings are summarized, and conclusions are drawn in Sec. V of this paper.

II. MATHEMATICAL BACKGROUND

The anisotropy associated with $\widetilde{u_i'' u_j''}$ and $\widetilde{\varepsilon}_{ij}$ can be analyzed in terms of anisotropy tensors b_{ij} and d_{ij}, which are defined as[5,25]

$$b_{ij} = \widetilde{u_i'' u_j''}/2\widetilde{k} - \delta_{ij}/3 \text{ and } d_{ij} = \widetilde{\varepsilon}_{ij}/2\widetilde{\varepsilon} - \delta_{ij}/3, \quad (1)$$

where $\widetilde{k} = \widetilde{u_i'' u_i''}/2$ and $\widetilde{\varepsilon} = \overline{\mu(\partial u_i''/\partial x_j)(\partial u_i''/\partial x_j)}/\overline{\rho} = \widetilde{\varepsilon}_{ii}/2$ are the turbulent kinetic energy and its dissipation rate, respectively.

It is worth noting that the derivation of the turbulent kinetic energy transport equation from the first principles yields the unclosed term, arising from the combined action of molecular diffusion of kinetic energy and viscous dissipation rate, which is given by[26]

$$T_V = \overline{u_i'' \frac{\partial \tau_{ij}}{\partial x_j}} = \underbrace{-\mu \overline{\frac{\partial u_i''}{\partial x_j}\frac{\partial u_i''}{\partial x_j}}}_{\overline{\rho}\widetilde{\varepsilon}}$$

$$+ \underbrace{\left[\overline{u_i'' \frac{\partial}{\partial x_k}\left(\mu \frac{\partial u_k''}{\partial x_i}\right)} - \frac{2}{3}\overline{u_i'' \frac{\partial}{\partial x_i}\left(\mu \frac{\partial u_k''}{\partial x_k}\right)} \right]}_{T_{VK}} + \frac{\partial}{\partial x_j}\left(\mu \frac{\partial \widetilde{k}}{\partial x_j}\right), \quad (2)$$

where $\tau_{ij} = \mu(\partial u_i/\partial x_j + \partial u_j/\partial x_i) - \delta_{ij}(2\mu/3)(\partial u_k/\partial x_k)$ is the component of the viscous stress tensor. It is clear from Eq. (2) that the expression of $\widetilde{\varepsilon}$ automatically arises out of the derivation of turbulent kinetic energy. It is also worth noting that T_{VK} disappears for incompressible (i.e., constant density) flows because $\partial u_k''/\partial x_k = 0$. Therefore, T_V reduces to $T_V = -\overline{\rho}\widetilde{\varepsilon} + \nabla \cdot (\mu\nabla\widetilde{k})$ for incompressible flows for which $k - \varepsilon$ model was originally developed. In the context of $k - \varepsilon$ modeling of turbulent premixed flames, the definition of viscous dissipation rate presented in this paper [i.e., $\widetilde{\varepsilon} = \overline{\mu(\partial u_i''/\partial x_j)(\partial u_i''/\partial x_j)}/\overline{\rho}$] is used. Separate models have been proposed for T_{VK},[21–23,26] and thus, the modeling of T_V translates to the closure of conventional dissipation rate. Wilcox[27] proposed an alternative definition of turbulence dissipation rate for compressible flows as

$$\widetilde{\varepsilon}_{comp} = \left[2\overline{\mu S_{ij}'' S_{ij}''} - 2/3\overline{\mu(\partial u_k''/\partial x_k)^2}\right]/\overline{\rho} = \widetilde{\varepsilon}_{sol} + \widetilde{\varepsilon}_{dil}, \quad (3)$$

where $S_{ij}'' = 0.5(\partial u_i''/\partial x_j + \partial u_j''/\partial x_i)$ is the fluctuating component of the strain rate tensor, $\widetilde{\varepsilon}_{sol} = \overline{\mu\omega_i''\omega_i''}/\overline{\rho}$ is the solenoidal part of the dissipation rate with ω_i'' is the ith component of the vorticity fluctuations, and $\widetilde{\varepsilon}_{dil} = \overline{4\mu(\partial u_i''/\partial x_i)(\partial u_j''/\partial x_j)}/3\overline{\rho}$ is the dissipation rate arising from the dilatation rate fluctuations $(\partial u_j''/\partial x_j)$. The value of $\widetilde{\varepsilon}_{dil}$ is identically zero for incompressible non-reacting flows and thus $\widetilde{\varepsilon}_{comp} = \widetilde{\varepsilon}_{sol}$ for incompressible flows, and consequently, the differences between $\widetilde{\varepsilon}_{comp}$ and $\widetilde{\varepsilon}_{sol}$ within the flame brush can be expected due to the non-zero $\widetilde{\varepsilon}_{dil}$ contribution within the flame. For the DNS data considered here, $\widetilde{\varepsilon}_{comp} = \widetilde{\varepsilon} + [\overline{\mu(\partial u_i''/\partial x_j)(\partial u_j''/\partial x_i)}]/\overline{\rho} - 2/3\overline{\mu(\partial u_k''/\partial x_k)^2}$ remains close to $\widetilde{\varepsilon}$ indicating that the net contribution of $[\overline{\mu(\partial u_i''/\partial x_j)(\partial u_j''/\partial x_i)}]/\overline{\rho} - 2/3\overline{\mu(\partial u_k''/\partial x_k)^2}$ remains small in comparison to the magnitude of $\widetilde{\varepsilon}$. Similar trends have been observed when compressible definition for $\widetilde{\varepsilon}_{ij}$ is used. This implies that using $\widetilde{\varepsilon}_{comp}$ instead of $\widetilde{\varepsilon}$ does not offer any major benefits for premixed flame–wall interaction cases considered in this work.

The tensors given by b_{ij} and d_{ij} are trace free (i.e., $b_{ii} = d_{ii} = 0$), but their second invariants are given by[5,25]

$$II_b = -b_{ij}b_{ji}/2 \quad \text{and} \quad II_d = -d_{ij}d_{ji}/2. \quad (4)$$

Similarly, the third invariants of b_{ij} and d_{ij} tensors are defined as[5,25]

$$III_b = b_{ij}b_{jk}b_{ki}/3 \quad \text{and} \quad III_d = d_{ij}d_{jk}d_{ki}/3. \quad (5)$$

The invariants given by Eqs. (4) and (5) in turn determine the eigenvalues of anisotropy tensors and these eigenvalues indicate different realizable limiting states of anisotropic turbulence in the following manner:[5,25]

- One-component (1C) limit: Here, one of the eigenvalues of $(\widetilde{u_i'' u_j''})$ or $\widetilde{\varepsilon}_{ij}$, as applicable, is non-zero and the eigenvalues of anisotropy b_{ij} and d_{ij} tensors are given by $[\lambda_1, \lambda_2, \lambda_3] = [2/3, -1/3, -1/3]$.
- Two-component (2C) axisymmetric limit: Here, two of the eigenvalues of $(\widetilde{u_i'' u_j''})$ or $\widetilde{\varepsilon}_{ij}$, as applicable, are non-zero and the eigenvalues of anisotropy b_{ij} and d_{ij} tensors are given by $[\lambda_1, \lambda_2, \lambda_3] = [1/6, 1/6, -1/3]$.
- Three-component (3C) isotropy limit: Here, three eigenvalues of $(\widetilde{u_i'' u_j''})$ or $\widetilde{\varepsilon}_{ij}$ are non-zero and equal, while the eigenvalues of anisotropy b_{ij} and d_{ij} tensors are given by $[\lambda_1, \lambda_2, \lambda_3] = [0, 0, 0]$.

The borders between these limits are characterized by the following intermediate relations:[5,25]

- Two-component limit, which is representative of ellipse-like (pancake) turbulence structures characterized by $\lambda_1 > \lambda_2$ and $\lambda_3 = 0$.
- An axisymmetric expansion, which is representative of rod-like turbulence structures characterized by $\lambda_1 > \lambda_2 = \lambda_3$.
- Axisymmetric compression, which is representative of disc-like turbulence structures characterized by $\lambda_1 = \lambda_2 > \lambda_3$.

All the realizable points fall within the Lumley triangle given by the aforementioned borders and vertices mentioned above.

A common model for $\widetilde{\varepsilon}_{ij}$ for non-reacting turbulent flow was proposed by Hanjalic and Launder[28] as

$$\widetilde{\varepsilon}_{ij} = f\widetilde{\varepsilon}_{ij}{}^a + (1-f)2\delta_{ij}\widetilde{\varepsilon}/3, \tag{6}$$

where $\widetilde{\varepsilon}_{ij}{}^a = (\widetilde{u_i'' u_j''}/\widetilde{k})\widetilde{\varepsilon}$, $f = (1 + Re_t/10)^{-1}$ is a bridging function with $Re_t = \widetilde{k}^2/\nu_R\widetilde{\varepsilon}$ being the turbulent Reynolds number and ν_R is the kinematic viscosity of the unburned gas. This model was previously shown to be ineffective for non-reacting turbulent boundary layer flows.[29] Antonia et al.[5] proposed alternative models for $\widetilde{\varepsilon}_{ij}$ as

$$\widetilde{\varepsilon}_{ij} = f_b\widetilde{\varepsilon}_{ij}{}^a + (1-f_b)\widetilde{\varepsilon}_{ij}{}^b, \tag{7}$$

where $f_b = \exp(-20A_b^2)$ with $A_b = 1 + 9(II_b + 3III_b)$ is a bridging function.[5,30] There are two modeling options for $\widetilde{\varepsilon}_{ij}{}^b$:[5,30,31]

$$\widetilde{\varepsilon}_{ij}{}^b = 2\widetilde{\varepsilon}(10Re_t^{-0.5}b_{ij} + \delta_{ij}/3), \tag{8a}$$

$$\widetilde{\varepsilon}_{ij}{}^b = 2\widetilde{\varepsilon}(b_{ij} - 2\alpha[(2II_b + 1/3)b_{ij} + (b_{ik}b_{kj} + 2II_b\delta_{ij}/3)] + \delta_{ij}/3), \tag{8b}$$

where α is a model parameter of the order of unity, which is taken to be 1.0 in the current analysis. The model expressions given by Eq. (6), Eq. (7) with Eq. (8a), and Eq. (7) with Eq. (8b) will henceforth be referred to as model 1, model 2, and model 3, respectively.

III. DNS DATABASE

For the purpose of the current analysis, the simulations are performed using a three-dimensional compressible code called SENGA+,[32] and the combustion chemistry is represented by a single-step Arrhenius type chemical reaction [unit mass of fuel + s unit mass of oxidizer $\rightarrow$ $(1+s)$ unit mass of products, where s is the stoichiometric oxidizer–fuel mass ratio] for the sake of computational economy. As the present analysis focuses primarily on the fluid-dynamical aspects of FWI, it is expected that the findings of this study will not be affected by the choice of the chemical mechanism. The chemical reaction affects the turbulence statistics only through the dilatation rate and it is discussed elsewhere[19,33–36] that the statistics of reactive scalar gradient, wall heat flux magnitude, and the flame quenching distance obtained from detailed chemical mechanism can be captured reasonably accurately by single-step chemistry. In the current analysis, stoichiometric methane–air premixed flames (i.e., $s = 4.0$) under atmospheric conditions are considered. The Lewis number of all the species is taken to be unity, and the unburned gas temperature T_R is taken to be 730 K, which yields a Zel'dovich parameter, $\beta = T_a(T_{ad} - T_R)/T_{ad}^2$ of 6.0 (where T_a, T_{ad}, and T_R is the activation, adiabatic, and reactant temperatures, respectively) and a heat release rate parameter of $\tau = (T_{ad} - T_R)/T_R = 2.3$. Standard values are taken for the Prandtl number, Pr, and the ratio of specific heat, γ (i.e., $Pr = 0.7$, $\gamma = 1.4$). The first- and second-order spatial derivatives in SENGA+ are calculated using a tenth-order finite difference central scheme for the internal grid points, but the order of accuracy gradually reduces to a second order for the non-periodic boundaries. A third-order Runge–Kutta scheme is used for explicit time advancement. The simulations in this analysis have been conducted in a configuration, where the turbulent boundary layer is formed on top of a chemically inert wall and the initial flow conditions for the reacting flow simulations have been generated using fully developed non-reacting turbulent channel flow solutions corresponding to $Re_\tau = u_{\tau,NR}h/\nu_R = 110$ and 180, where $u_{\tau,NR} = \sqrt{|\tau_{w,NR}|/\rho_R}$ and $\tau_{w,NR}$ are the friction velocity and wall shear stress for the non-reacting channel flow, respectively, ρ_R is the unburned gas density, and h is the channel half height corresponding to the non-reacting fully developed channel flow solution.

The computational domain size for the reacting cases at both $Re_\tau = 110$ and 180 are taken to be $10.69h \times 1.33h \times 4h$ and equidistant cartesian grids of $1920 \times 240 \times 720$ and $3200 \times 400 \times 1200$ are used for $Re_\tau = 110$ and 180, respectively. These grids ensure that $y_{NR}^+ = (\rho_R u_{\tau,NR}y)/\mu_R$ for the wall adjacent grid points remain smaller than 0.6, which satisfies the criteria proposed by Moser et al.[37] for simulating turbulent boundary layers, and at least eight grid points are accommodated within the thermal flame thickness $\delta_{th} = (T_{ad} - T_R)/\max |\nabla T|_L$ (where T is the instantaneous dimensional temperature). The non-reacting flow simulations have been benchmarked with respect to previous DNS by other researchers,[38] and it is shown elsewhere[19,36,39] that an excellent agreement is obtained. It should be recognized here that the bulk and friction Reynolds numbers for the simulations performed in this work are comparable to the recent state-of-the-art experiments performed for FWI.[40]

In all of the reacting flow simulations, periodic boundary conditions are used for both streamwise (i.e., x-coordinate) and spanwise (i.e., z-coordinate) directions, and a pressure gradient (i.e., $-\partial p/\partial x = \rho u_{\tau,NR}^2/h$, where p is the pressure) has been imposed in the streamwise direction.[19,36,39] A no-slip impenetrable, inert (i.e., velocity components in wall normal and tangential directions are zero and mass flux in the wall-normal direction vanishes) wall boundary condition is implemented at $y = 0$, and an isothermal wall boundary condition (i.e., $T_w = T_R$) is imposed for the temperature at the wall. A

partially nonreflecting boundary is specified at $y/h = 1.33$. The schematic of the flow configuration is presented in Fig. 1. For both $Re_\tau = 110$ and 180 cases, an unstretched steady state 1D laminar flame solution has been interpolated onto the 3D grid in such a manner that the reaction progress variable $c = (Y_{FR} - Y_F)/(Y_{FR} - Y_{FP})$ (where the subscripts R and P represent the fresh reactant and fully burned products, respectively) takes a value of 0.5, at $y/h \approx 0.85$ such that the reactant side faces the wall, whereas the burned gas side faces the outflow boundary of the domain. The ratio of the laminar burning velocity, S_L, and non-reacting flow friction velocity, $u_{\tau,NR}$, is taken to be 0.7 for all cases considered here. The simulations have been continued for a maximum of 2.0 flow through time based on the maximum streamwise mean velocity. The flames propagate toward the wall and eventually quench due to heat loss through the wall over the simulation time, but the boundary layer does not evolve significantly.[19,36,39] The Reynolds and Favre averaged quantities in this configuration have been evaluated by spatial averaging the quantities of interest in the periodic directions (i.e., x–z planes) for a given time instant and thus the averaged quantities only vary in the y-direction.

IV. RESULTS AND DISCUSSION

The instantaneous views of $c = 0.8$ isosurface for different normalized times at $t/t_f = 3.99$, 13.12, and 16.27 in the case of $Re_\tau = 110$, and $t/t_f = 7.89$, 16.75, and 20.11 for $Re_\tau = 180$ cases are shown in Fig. 2, where $t_f = \delta_{th}/S_L$ is the chemical time scale. The distributions of the normalized vorticity magnitude, $\Omega = \sqrt{\omega_i \omega_i} \times h/u_{\tau,NR}$, at $z/h = 4.0$ are also shown in Fig. 2. The choice of $c = 0.8$ is driven by the fact that the peak value of the reaction rate of the reaction progress variable is obtained for $c \approx 0.8$ for the unstretched steady laminar premixed flame so this isosurface can be considered as the flame surface. Figure 2 shows that the flame surface becomes wrinkled due to the interaction of turbulent shear and vortical motion within the boundary layer, but these wrinkles eventually quench when they come in the vicinity of the wall (i.e., the normalized minimum quenching distance is $y_Q/\delta_Z = 1.71$ and 1.72 for $Re_\tau = 110$ and 180 turbulent cases, with $\delta_Z = \alpha_{T_0}/S_L$ and α_{T_0} being the Zel'dovich flame thickness and thermal diffusivity in the unburned gas, respectively, and y_Q is the wall-normal quenching distance of the temperature isosurface corresponding to the peak reaction rate of the unstretched laminar premixed flame) due to the heat loss. This quenching is reflected in the fragmented flame surface at later times in Fig. 2. The presence of the flame within turbulent boundary layers gives rise to a predominantly
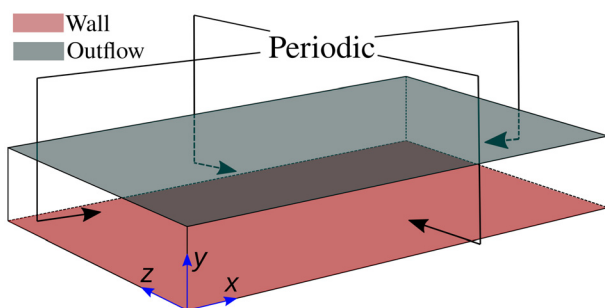

FIG. 1. Schematic of the computational domain used for head-on quenching of the statistically planar flame across a turbulent boundary layer.
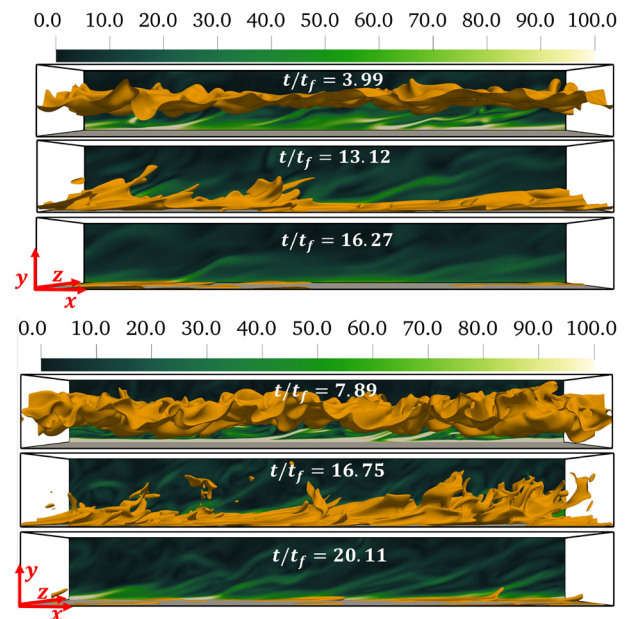

FIG. 2. Head-on quenching for the premixed flame case with $Re_\tau = 110$ (top) and 180 (bottom) at different t/t_f. The isosurface colored in yellow represents $c = 0.8$. The instantaneous normalized vorticity magnitude $\Omega = \sqrt{\omega_i \omega_i} \times h/u_{\tau,NR}$ is shown on the x–y plane at $z/h = 4$. The gray surface denotes the wall.

positive dilatation rate (i.e., $\partial u_i/\partial x_i > 0$), which in turn affects the turbulence statistics due to flame normal acceleration resulting from thermal expansion.[19,39] This has implications for the distribution of $\widetilde{u_i'' u_j''}$ and $\widetilde{\varepsilon}_{ij}$ components within turbulent boundary layers analyzed here. In this configuration, only $\widetilde{u_1'' u_1''}$, $\widetilde{u_2'' u_2''}$, $\widetilde{u_3'' u_3''}$, and $\widetilde{u_1'' u_2''}$ assume non-zero values for the Reynolds stress tensor, whereas $\widetilde{\varepsilon}_{11}$, $\widetilde{\varepsilon}_{22}$, $\widetilde{\varepsilon}_{33}$, and $\widetilde{\varepsilon}_{12}$ are the non-zero components of the viscous dissipation rate, $\widetilde{\varepsilon}_{ij}$, tensor.

As the present configuration represents an unsteady FWI configuration, the statistics related to the non-zero components of $\widetilde{u_i'' u_j''}$ and $\widetilde{\varepsilon}_{ij}$ will henceforth be presented at $t/t_f = 3.99$, 13.12, and 16.27 for $Re_\tau = 110$ and at $t/t_f = 7.89$, 16.75, and 20.11 for $Re_\tau = 180$ cases, which correspond to the normalized wall normal distance of $y/h = 0.72$, 0.06, and 0.03 for non-dimensional Favre-averaged temperature $\widetilde{\theta} = (\widetilde{T} - T_0)/(T_{ad} - T_0) = 0.5$ isosurface for each Re_τ, respectively. For the following discussion, these time instants will be considered for the purpose of further analysis because these conditions are representative of the situations (i) when the flame is away from the wall and thus without any wall influence, (ii) when the flame is interacting with the wall, and (iii) when the flame is mostly quenched. These can further be substantiated by the distributions of Favre-averaged values of the reaction progress variable $\widetilde{c}$ and non-dimensional temperature $\widetilde{\theta}$ with the normalized wall normal distance y/h, as shown in Fig. 3, which shows that $\widetilde{c} = \widetilde{\theta}$ is maintained away from the wall, as expected for unity Lewis number conditions in low Mach number flows. However, it can be seen from Fig. 3 that the coupling between $\widetilde{c}$ and $\widetilde{\theta}$ is lost during FWI due to different wall boundary conditions for c and θ (i.e., $\partial c/\partial y|_w = 0$ and $\theta|_w = 0$), which is consistent with several previous studies.[41–43] After flame quenching,
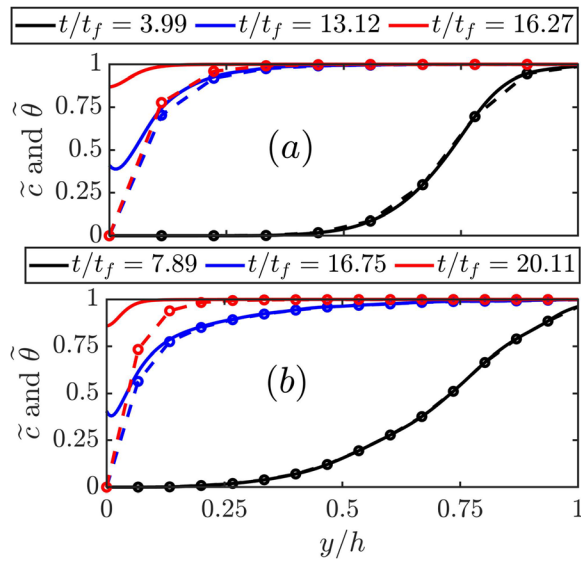
FIG. 3. Distributions of Favre-averaged values of reaction progress variable $\widetilde{c}$ (solid lines) and non-dimensional temperature $\widetilde{\theta}$ (dashed lines with symbols) with y/h at different time instants for $Re_\tau =$ (a) 110 and (b) 180.

burned gas diffuses toward the wall and the unburned gas close to the wall diffuses away from it, and accordingly the value of $\widetilde{c}$ increases from 0.0 with the progress of FWI, which is also consistent with previous experimental[44,45] and computational[41–43] findings. It can further be appreciated from Figs. 2 and 3 that burned gas increasingly occupies a major part of the turbulent boundary layer with the progress of FWI, which has implications on the distributions of $\widetilde{u_i'' u_j''}$ and $\widetilde{\varepsilon}_{ij}$ components.

The distributions of $[\widetilde{u_1'' u_1''}, \widetilde{u_2'' u_2''}, \widetilde{u_3'' u_3''}, \widetilde{u_1'' u_2''}, \widetilde{k}]/u_{\tau,NR}^2$ and $[\widetilde{\varepsilon}_{11}, \widetilde{\varepsilon}_{22}, \widetilde{\varepsilon}_{33}, \widetilde{\varepsilon}_{12}, \widetilde{\varepsilon}] \times \nu_{NR}/u_{\tau,NR}^4$ with y/h at different stages of FWI are shown in Figs. 4 and 5, respectively, for both Re_τ=110 and 180 cases. Figures 4 and 5 show that $\widetilde{u_1'' u_1''}$ and $\widetilde{\varepsilon}_{11}$ are the dominant contributors of $\widetilde{k}$ and $\widetilde{\varepsilon}$, respectively, which are consistent with the expected behavior in turbulent boundary layers. However, a comparison between Figs. 3 and 4 reveals that the differences in $\widetilde{u_1'' u_1''}$ and $\widetilde{k}$ between the premixed flame and the fully developed non-reacting channel flow profiles are obtained within the flame brush (e.g., $0.1 \leq \widetilde{c} \leq 0.9$), where the effects of thermal expansion due to heat release are strong when the flame remains away from the wall (e.g., $t/t_f = 3.99$ and 7.89 for the $Re_\tau = 110$ and 180 cases, respectively). The differences for $\widetilde{u_1'' u_1''}$ and $\widetilde{k}$ between the reacting and non-reacting cases increase with the progress of flame quenching. When the flame starts to interact with the wall (e.g., $t/t_f = 13.12$ and 16.75 for the $Re_\tau = 110$ and 180
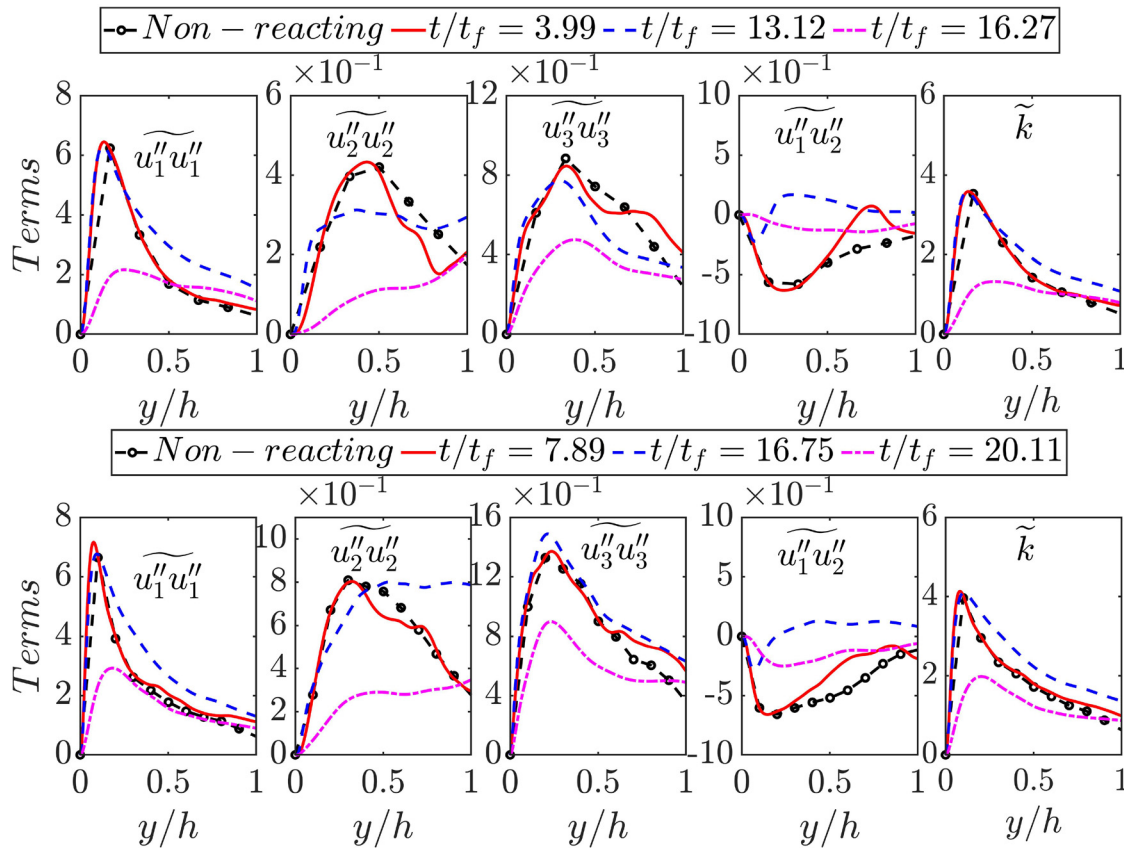

FIG. 4. Distributions of $[\widetilde{u_1'' u_1''}, \widetilde{u_2'' u_2''}, \widetilde{u_3'' u_3''}, \widetilde{u_1'' u_2''}$, and $\widetilde{k}]/u_{\tau,NR}^2$ with y/h at different t/t_f for $Re_\tau = 110$ (first row) and 180 (second row).

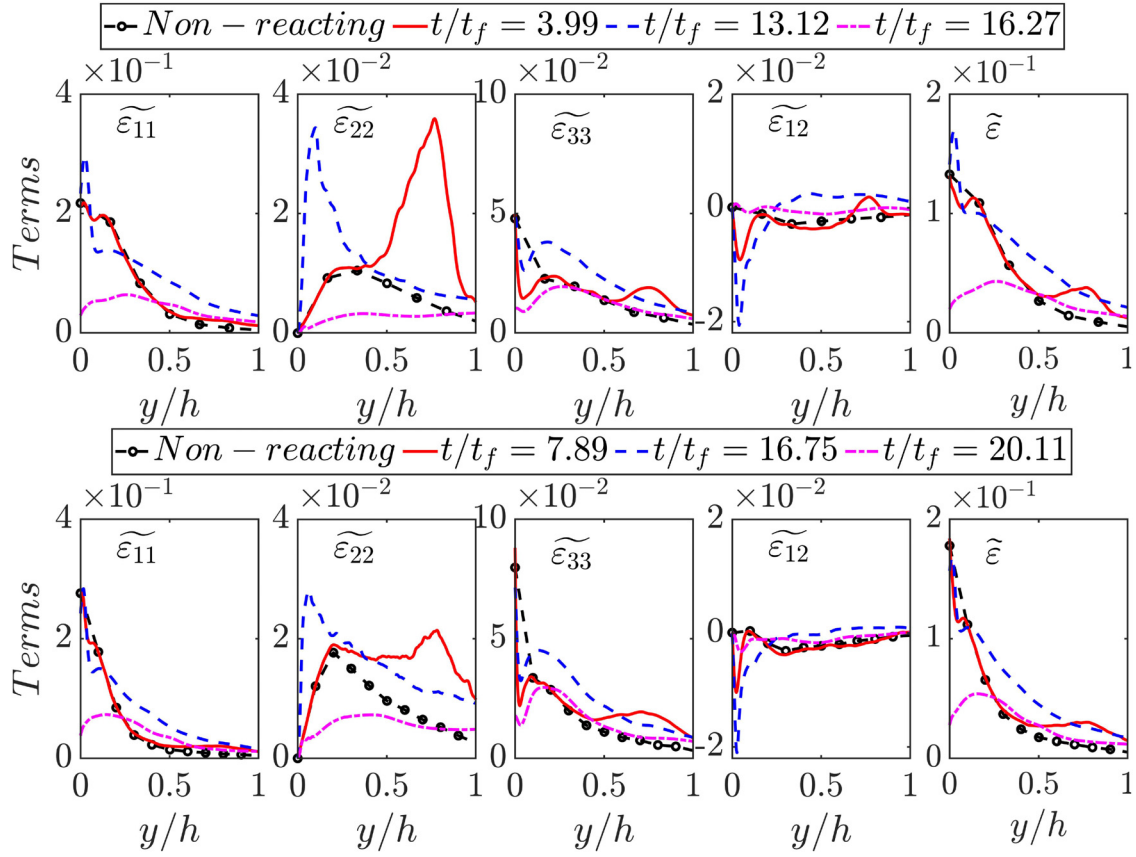**FIG. 5.** Distributions of $[\widetilde{\varepsilon}_{11}, \widetilde{\varepsilon}_{22}, \widetilde{\varepsilon}_{33}, \widetilde{\varepsilon}_{12},$ and $\widetilde{\varepsilon}] \times \nu_{NR}/u_{\tau,NR}^4$ with y/h at different t/t_f for $Re_\tau = 110$ (first row) and 180 (second row).

cases, respectively), $\widetilde{u_2'' u_2''}$ and $\widetilde{u_1'' u_2''}$ are significantly affected by the heat release as the flame normal vector in a mean sense aligns mostly with the wall-normal direction, and thus, the thermal expansion effects are mostly felt in the Reynolds stress components involving velocity fluctuations in the wall-normal direction. The redistribution of Reynolds stresses gives rise to the alteration of $\widetilde{u_3'' u_3''}$ in the reacting cases in comparison to the corresponding non-reacting flow profiles. The alterations of $\widetilde{u_2'' u_2''}$ and $\widetilde{u_3'' u_3''}$ due to thermal expansion and momentum redistribution at the early stages of HOQ are masked by the dominant contribution of $\widetilde{u_1'' u_1''}$ toward $\widetilde{k} = \widetilde{u_i'' u_i''}/2$. Moreover, a comparison between Figs. 3 and 4 reveals that $\widetilde{u_1'' u_2''}$ assumes positive values within the flame brush and in the burned gas for the early stages of FWI (e.g., $t/t_f = 13.12$ and 16.75 for the $Re_\tau = 110$ and 180 cases, respectively), whereas $\widetilde{u_1'' u_2''}$ for fully developed non-reacting channel flow assumes negative values. Thus, the positive values of $\widetilde{u_1'' u_2''}$ are indicative of counter-gradient behavior as $\partial \widetilde{u}_1/\partial x_2 > 0$ is obtained throughout the boundary layer. The quantity $\widetilde{u_i'' u_j''}$ can be expressed as[16]

$$\widetilde{u_i'' u_j''} = \widetilde{c}(1 - \widetilde{c})\left[(\overline{u}_i)_P - (\overline{u}_i)_R\right]\left[(\overline{u}_j)_P - (\overline{u}_j)_R\right] \\ + (1 - \widetilde{c})\overline{(u_i' u_j')}_R + \widetilde{c}\,\overline{(u_i' u_j')}_P + \mathcal{O}(\gamma_c), \quad (9)$$

where $(\overline{q})_R$ and $(\overline{q})_P$ are the conditional mean values in unburned reactants and products of a general quantity q and $\mathcal{O}(\gamma_c)$ is the contribution of the burning mixture. The counter-gradient behavior of $\widetilde{u_1'' u_2''}$ occurs when the contribution due to velocity jump across the flame brush [i.e., which leads to positive values for the first term on the right-hand side of Eq. (9)] dominates over the turbulent velocity fluctuation contributions [i.e., second and third terms on the right-hand side of Eq. (9)],[16,46] but a gradient type of transport is obtained when fluid turbulence contributions [i.e., second and third terms on the right-hand side of Eq. (9)] overwhelm the effects of flame normal acceleration due to thermal expansion [i.e., first term on the right-hand side of Eq. (9)]. Therefore, a gradient type of behavior (negative value in this configuration) for $\widetilde{u_1'' u_2''}$ is observed for both cases when the flames are at an advanced stage of quenching (e.g., $t/t_f = 16.27$ and 20.11 for the $Re_\tau = 110$ and 180 cases, respectively). However, the magnitudes of $\widetilde{u_1'' u_2''}$ remain greater than the corresponding non-reacting values even when the gradient type of transport is obtained at the advanced stage of HOQ. At advanced stages of HOQ (e.g., $t/t_f = 16.27$ and 20.11 for the $Re_\tau = 110$ and 180 cases, respectively), the turbulent boundary layer is filled by the burned gas and the high kinematic viscosity in the burned gas gives rise to a significant drop in the magnitudes of all Reynolds stress components and $\widetilde{k}$ due to the dampening of turbulent
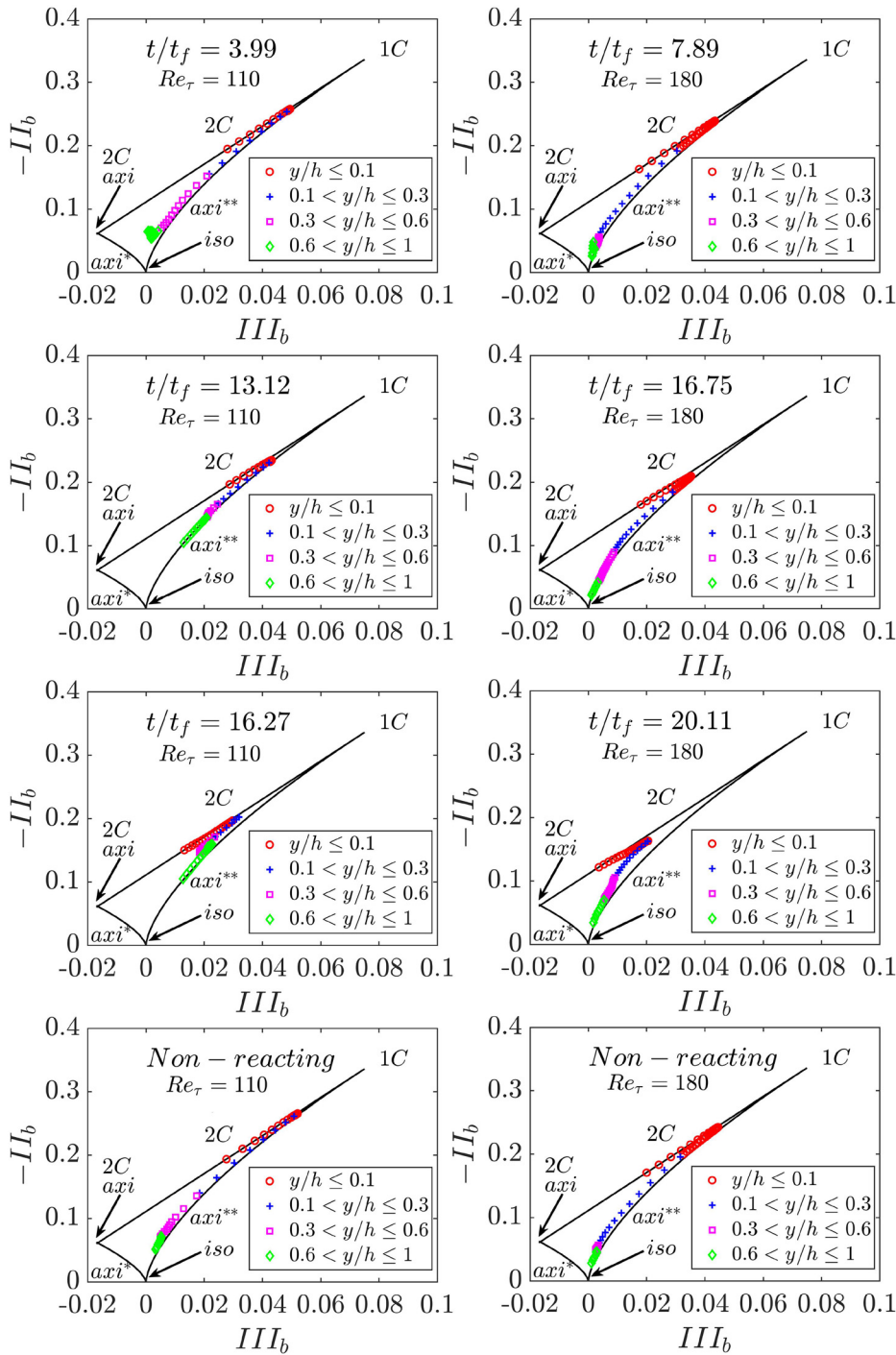
FIG. 6. Plots of $-II_b$ vs III_b in the form of the Lumley triangle for $Re_\tau = 110$ (first column) and 180 (second column) at different t/t_f. Note axi^* represents axisymmetric contraction and axi^{**} represents axisymmetric expansion.

fluid motion. However, $\widetilde{u_1''u_1''}$ continues to be the major contributor to $\widetilde{k} = \widetilde{u_i''u_i''}/2$ even at the advanced stages of HOQ (e.g., $t/t_f = 16.27$ and 20.11 for the $Re_\tau = 110$ and 180 cases, respectively), which is characteristic of wall-induced shear flows within turbulent boundary layers under imposed pressure gradient.[5,29]

Similar to the Reynolds stress components, $\widetilde{\varepsilon}_{11}$ acts as the dominant contributor to $2\widetilde{\varepsilon} = \widetilde{\varepsilon}_{ii}$ for both Re_τ cases considered here. Moreover, the differences in $\widetilde{\varepsilon}_{ij}$ between non-reacting and reacting cases are obtained only within the flame brush and in the burned gas side, where the effects of thermal expansion

are strong at the early stages of HOQ. By contrast, at the advanced stages of HOQ, the decay of turbulence due to the strengthening of viscous damping within the burned gas leads to significant drops in the magnitudes of $\widetilde{\varepsilon}_{ij}$ and $\widetilde{\varepsilon}$ in comparison to the corresponding values obtained for non-reacting fully developed channel flows. However, $\widetilde{\varepsilon}_{11}$ continues to act as the dominant contributor to $2\widetilde{\varepsilon} = \widetilde{\varepsilon}_{ii}$ for both Re_{τ} cases even at the advanced stages of HOQ, which is once again characteristic of wall-bounded turbulent boundary layer flows under imposed pressure gradient.[5,29]
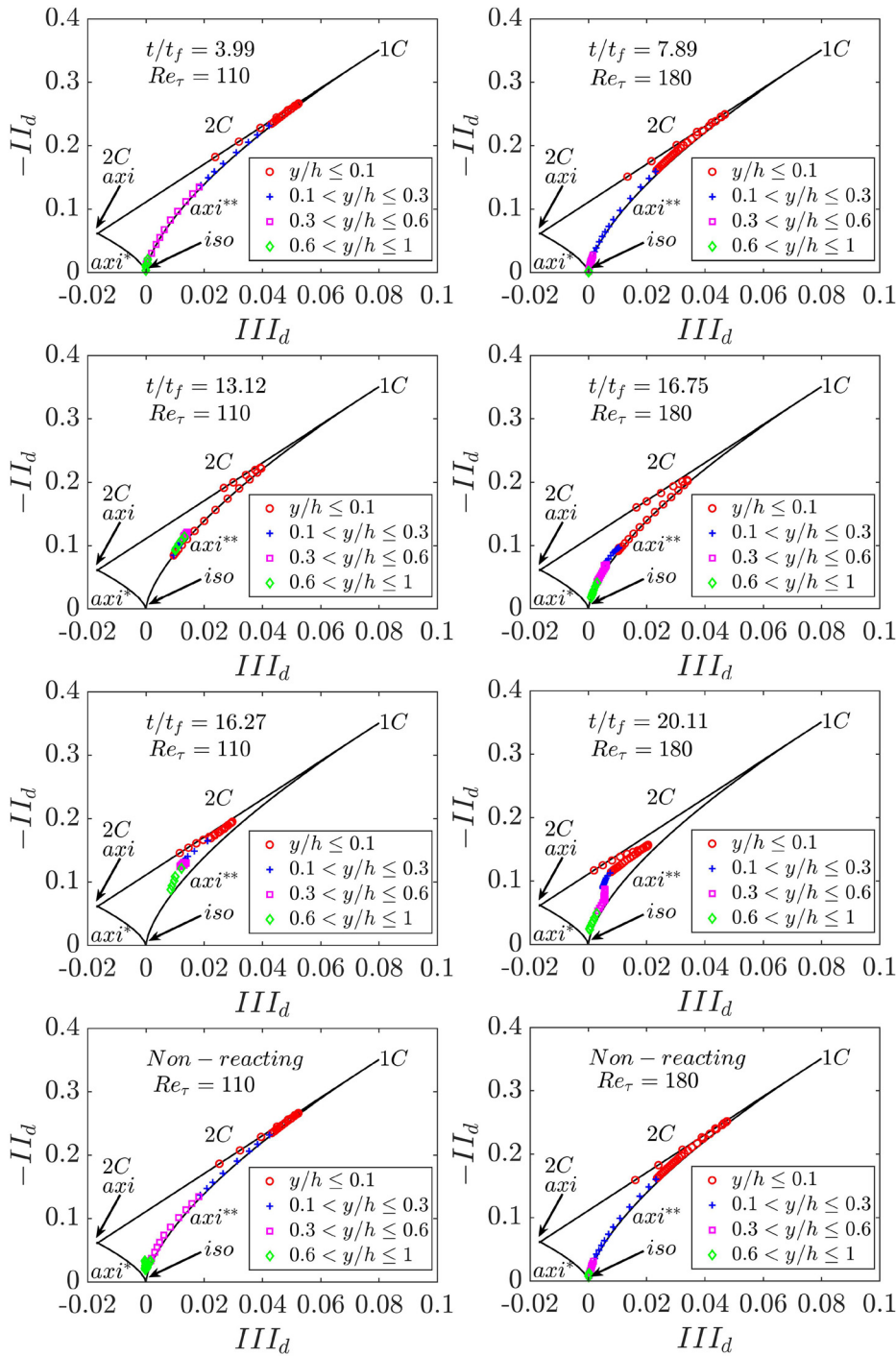

FIG. 7. Plots of $-II_d$ vs III_d in the form of the Lumley triangle for $Re_{\tau} = 110$ (first column) and 180 (second column) at different t/t_f. Note *axi** represents axisymmetric contraction and *axi*** represents axisymmetric expansion.

The findings from Figs. 4 and 5 suggest that $\widetilde{u_i'' u_j''}$ and $\widetilde{\varepsilon}_{ij}$ tensors demonstrate a significant amount of anisotropy at all stages of FWI in this configuration. The different states of anisotropy can be characterized in terms of the plots of $-II_b$ vs III_b and $-II_d$ vs III_d in the form of the Lumley triangle for the Reynolds stress tensor and dissipation rate tensor, respectively, which are shown in Figs. 6 and 7 at different time instants for both $Re_\tau = 110$ and 180 cases, respectively. The corresponding plots for non-reacting isothermal fully developed channel flow are also shown in Figs. 6 and 7, which show that the two-component elliptic behavior is obtained close to the wall for non-reacting fully developed channel flows, which is consistent with the fact that $2\widetilde{k}$ is dominated by $\widetilde{u_1'' u_1''}$ and $\widetilde{u_3'' u_3''}$ contributions. Similarly, $2\widetilde{\varepsilon}$ is dominated by $\widetilde{\varepsilon}_{11}$ and $\widetilde{\varepsilon}_{33}$ contributions. This is followed by a tendency toward the one-component limit for small values of y/h (due to the peak value of predominant $\widetilde{u_1'' u_1''}$ and $\widetilde{\varepsilon}_{11}$ at around $y/h \approx 0.1$) before exhibiting axisymmetric expansion [i.e., $\widetilde{u_1'' u_1''} > (\widetilde{u_2'' u_2''} + \widetilde{u_3'' u_3''})$ and $\widetilde{\varepsilon}_{11} > (\widetilde{\varepsilon}_{22} + \widetilde{\varepsilon}_{33})$] and finally tending toward isotropy close to $y/h = 1.0$. The same qualitative behavior is obtained for the reacting cases when the flames remain away from the wall, but the tendency toward isotropy close to $y/h \approx 1.0$ is stronger for the $Re_\tau = 180$ case than in the $Re_\tau = 110$ case, which is consistent with the greater tendency toward isotropy for higher values of the Reynolds number.

It can further be seen from Figs. 6 and 7 that the tendency toward isotropy close to $y/h = 1.0$ at later stages of HOQ (e.g., $t/t_f = 16.75$) becomes weaker than at earlier times (e.g., $t/t_f = 3.99$) for the $Re_\tau = 110$ case and two-component-elliptical and axisymmetric expansion behaviors are mostly obtained for this case. By contrast, in the case of HOQ for $Re_\tau = 180$, the behaviors of the second and third invariants remain qualitatively similar to the non-reacting case at all stages of FWI and the tendency toward isotropy is obtained close to $y/h \approx 1.0$. In this respect, it is worth noting that Durbin and Speziale[47] indicated even in the limit of the infinite value of Reynolds number the true isotropy is inconsistent with Navier–Stokes equations in the presence of mean shear rate, as is the case for turbulent boundary layer flows.

Lumley[48] suggested that $d_{ij}/b_{ij} \sim (\lambda_T/u')/(l/u') \sim Re_t^{-0.5}$, where λ_T and l are the Taylor microscale and integral length scale, respectively, but this scaling is rendered invalid at $Re_t = 0$ (at the wall) and $d_{ij} \neq 0$ is obtained for $Re_t \to \infty$. Therefore, a Re_t based blending function in Eq. (6) may not be suitable for turbulent boundary layers. It was demonstrated in previous studies[5,29] that a strictly linear relation is not obtained between $Re_t^{-0.5}b_{ij}$ and d_{ij} in the case of non-reacting turbulent boundary layer flows, which has also been observed for both non-reacting and reacting cases considered here, and is shown in Fig. 8.

The predictions of $\widetilde{\varepsilon}_{11}, \widetilde{\varepsilon}_{22}, \widetilde{\varepsilon}_{33}$, and $\widetilde{\varepsilon}_{12} \times \nu_{NR}/u_{\tau,NR}^4$ according to Eq. (6), Eq. (7) [with Eq. (8a)], and Eq. (7) [with Eq. (8b)] (i.e., model 1, model 2, and model 3) are compared with the corresponding values from the DNS data in Figs. 9 and 10, for $Re_\tau = 110$ and 180 cases, respectively, which also shows model 1 does not adequately capture both qualitative and quantitative behaviors of $\widetilde{\varepsilon}_{11}, \widetilde{\varepsilon}_{22}, \widetilde{\varepsilon}_{33}$, and $\widetilde{\varepsilon}_{12}$ extracted from the DNS data. Model 2 and model 3 reasonably capture the behaviors of $\widetilde{\varepsilon}_{11}$ for both non-reacting and reacting cases considered here, but the quantitative agreement is less satisfactory for $\widetilde{\varepsilon}_{22}$, $\widetilde{\varepsilon}_{33}$, and $\widetilde{\varepsilon}_{12}$. Moreover, model 2 yields a wrong sign of $\widetilde{\varepsilon}_{22}$ close to the centerline, where the effects of thermal expansion are strong in the reacting case with $Re_\tau = 110$ at $t/t_f = 3.99$ because the negative contribution of $10Re_t^{-0.5} b_{22}$ overcomes $1/3$ in Eq. (8a), but this problem disappears in the premixed FWI case with $Re_\tau = 180$. The better performance of model 3 than model 2 originates because $A_b = 1 + 9(II_b + 3III_b)$ in f_b accounts for the departure from the two-component limit (where $A_b = 0$). The model by Hallback et al.[31] utilizes the local anisotropy behavior in terms of II_b and III_b and satisfies (a) the symmetry with respect to i and j, (b) $d_{ii} = 0$, and (c) in the homogeneous two-component limit yields ($d_{m^*m^*} = b_{m^*m^*} = -1/3$, where $*$ indicates no summation). Thus, model 3 is more successful than other models in predicting the behavior for the diagonal components in $\widetilde{\varepsilon}_{ij}$, and the model performance has been found to improve with an increase in Re_t. However, the behavior for the off diagonal components of $\widetilde{\varepsilon}_{ij}$ is better predicted by model 1. Therefore, model 3
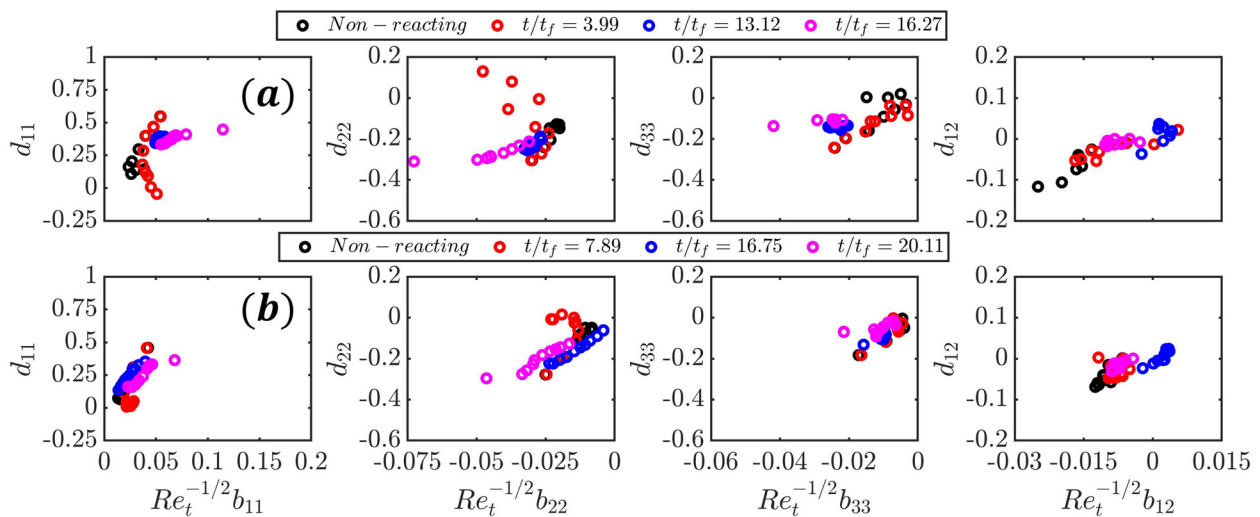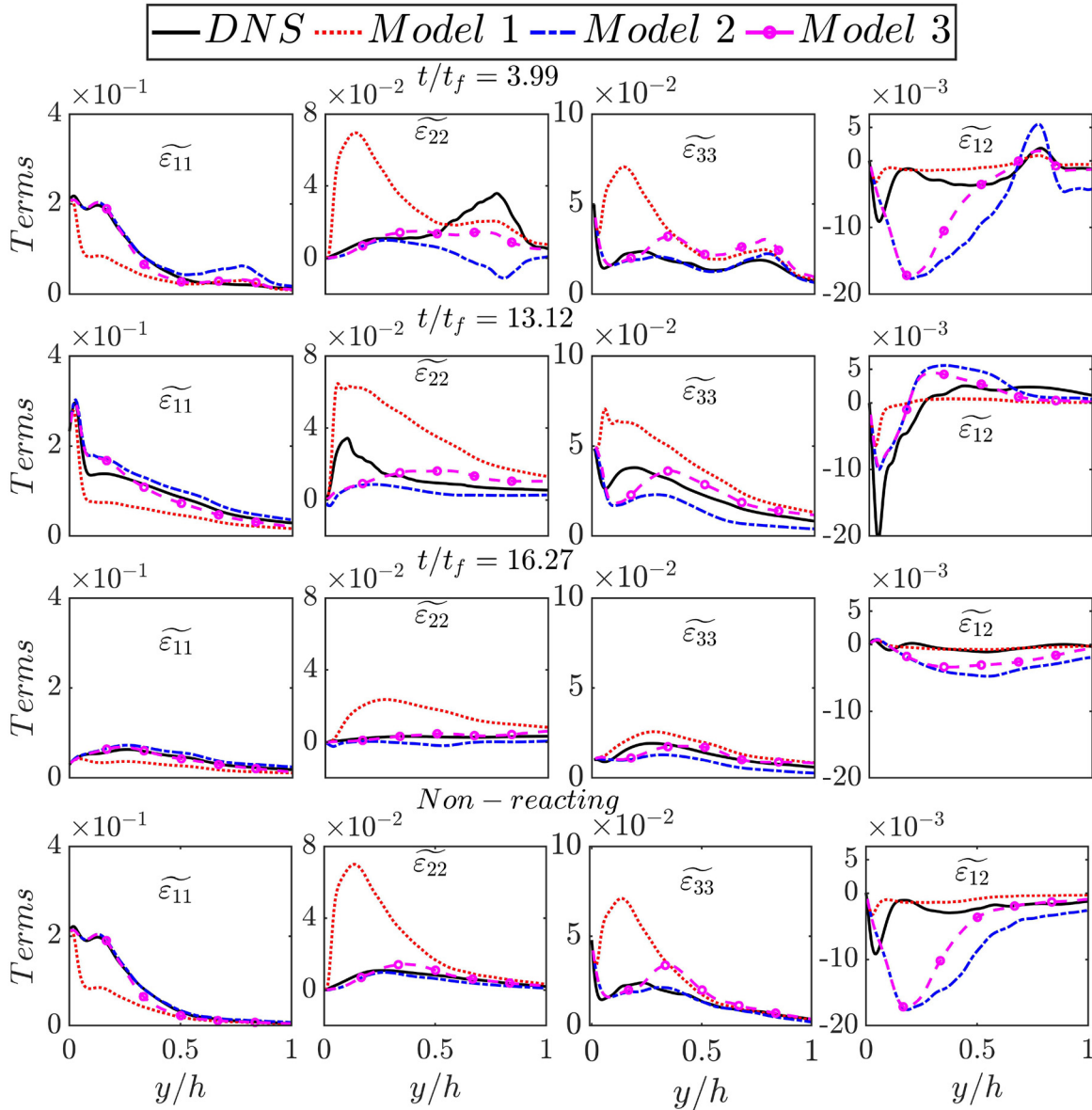
FIG. 8. Variations of d_{ij} with $Re_t^{-0.5}b_{ij}$ at different time instants for $Re_\tau =$ (a) 110 and (b) 180.

FIG. 9. Predictions of model 1 [i.e., Eq. (6)], model 2 [i.e., Eq. (7) with f_b given by Eq. (8a)], and model 3 [i.e., Eq. (7) with f_b given by Eq. (8b)] for $\widetilde{\varepsilon}_{11}$, $\widetilde{\varepsilon}_{22}$, $\widetilde{\varepsilon}_{33}$, and $\widetilde{\varepsilon}_{12}$ $\times \nu_{NR}/u_{\tau,NR}^4$ with the corresponding DNS data at different t/t_f for $Re_\tau = 110$.

can be considered for approximating the diagonal components of $\widetilde{\varepsilon}_{ij}$ and model 1 can be used for closing the off diagonal components of $\widetilde{\varepsilon}_{ij}$ in the Reynolds stress transport closure. This suggests that there is a further scope for improvement in the modeling of $\widetilde{\varepsilon}_{ij}$. This behavior for model performance is qualitatively similar to that reported by Antonia et al.[5] in the case of non-reacting boundary layer flows. Note that according to models 1–3 the trace of $\widetilde{\varepsilon}_{ij}$ yields $2\widetilde{\varepsilon}$, and thus, $\widetilde{\varepsilon}$ is not shown in Figs. 9 and 10. It is worth noting that models 1–3 were originally proposed for non-reacting flows, but the reasonable performance of model 3 in reacting flows in the cases considered here

originates principally due to the fact that the effects of thermal expansion are implicitly accounted for in the invariants of the Reynolds stress tensor.

A high-fidelity modeling of dissipation rate tensor allows for accurate predictions of turbulent kinetic energy, $\widetilde{k}$, and its dissipation rate, $\widetilde{\varepsilon}$, which are often input parameters in the closures of flame surface density[17] and scalar dissipation rate[18] models, needed for the accurate closure of the mean reaction rate. As mentioned before, Boussinesq's hypothesis is not able to predict the anisotropic behaviors of normal Reynolds stresses and, thus, accurate closures for $\widetilde{\varepsilon}_{ij}$ allow
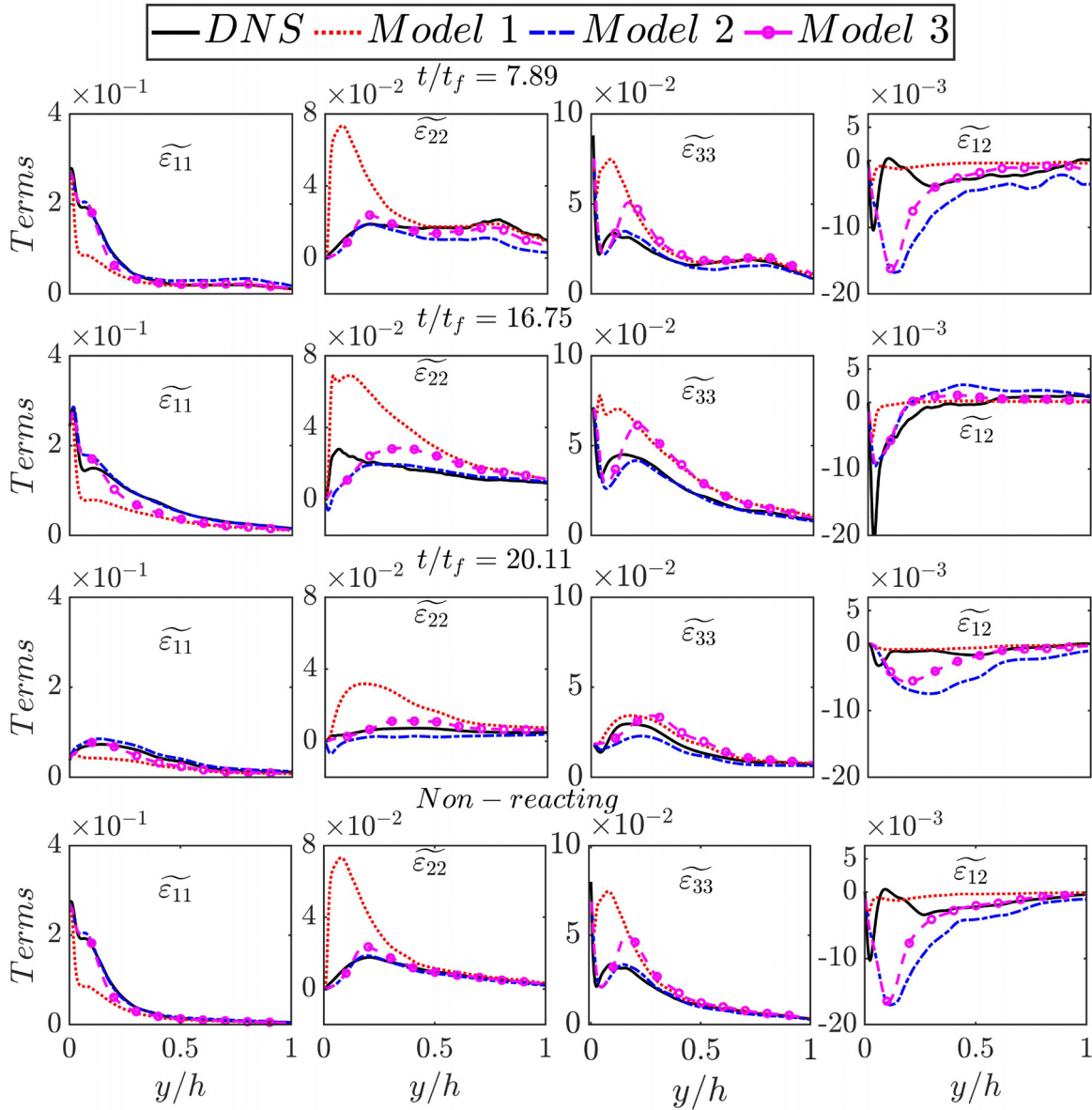
FIG. 10. Predictions of model 1 [i.e., Eq. (6)], model 2 [i.e., Eq. (7) with f_b given by Eq. (8a)], and model 3 [i.e., Eq. (7) with f_b given by Eq. (8b)] for $\widetilde{\varepsilon}_{11}$, $\widetilde{\varepsilon}_{22}$, $\widetilde{\varepsilon}_{33}$, and $\widetilde{\varepsilon}_{12}$ $\times \nu_{NR}/u^4_{\tau,NR}$ with the corresponding DNS data at different t/t_f for $Re_\tau = 180$.

for higher fidelity in the prediction of $\widetilde{u''_i u''_j}$ and consequently $\widetilde{k}$, which in turn indirectly affect the closures of flame surface density and scalar dissipation rate in premixed turbulent flames. Thus, an improved closure of $\widetilde{\varepsilon}_{ij}$ will not only affect the predictions of turbulent kinetic energy $\widetilde{k}$ and its dissipation rate $\widetilde{\varepsilon}$, but will give rise to more accurate predictions of the mean reaction rate as well.

V. CONCLUSIONS

The interrelation between Reynolds stresses and their dissipation rates during head-on quenching of premixed flames within turbulent boundary layers has been analyzed using DNS data for friction Reynolds numbers, Re_τ, of 110 and 180. It has been found that both Reynolds stresses and their dissipation rates show significant deviations from the corresponding non-reacting flow profiles within the flame brush and in the burned gas region. This behavior is particularly strong for the components in the wall-normal direction because the mean direction of flame normal acceleration due to thermal expansion aligns with the wall-normal direction in this configuration. The anisotropy of the Reynolds stress tensor and its dissipation rate tensor is found to be qualitatively similar but the anisotropic behavior

corresponding to axisymmetric expansion is relatively strong in the premixed flame case with $Re_\tau = 110$, and this anisotropy weakens with increasing friction Reynolds number. Despite the qualitative similarities in the anisotropy behavior of the Reynolds stress tensor and its dissipation rate tensor, the components of the corresponding anisotropy tensors cannot be assumed to be linearly related, and thus, the models based on this assumption are not successful in capturing the diagonal components of the viscous dissipation rate tensor but the agreement is found to be relatively better for the non-diagonal components. By contrast, a model, which accounts for the statistical behaviors of the invariants of the anisotropy tensor of Reynolds stresses and satisfies the limiting conditions for isotropy and two-component limit explicitly, has been found to reasonably capture the diagonal components of $\widetilde{\varepsilon}_{ij}$ tensor but the quantitative prediction suffers for the components in the wall-normal direction for small values of Re_τ. However, the performance of this model improves with an increase in Re_τ, and thus, this model can be used for modeling the diagonal components of $\widetilde{\varepsilon}_{ij}$ for the Reynolds stress closure in the context of FWI modeling under the hybrid RANS/LES framework. Although the simplification of chemistry made in this analysis is unlikely to affect the turbulence statistics presented here, further validation of the performance of the models in the presence of detailed chemistry and transport will be necessary. Finally, the model identified to provide satisfactory performance based on DNS data will also need to be implemented in hybrid RANS/LES of FWI for *a posteriori* model assessment, which will form the basis of future investigations.

ACKNOWLEDGMENTS

AUTHOR DECLARATIONS
Conflict of Interest

The authors have no conflicts to disclose.

Author Contributions

Umair Ahmed: Conceptualization (equal); Data curation (equal); Formal analysis (equal); Funding acquisition (supporting); Methodology (equal); Software (equal); Supervision (equal); Writing – review & editing (equal). **Sanjeev Ghai:** Data curation (equal); Formal analysis (equal); Software (equal); Visualization (equal); Writing – review & editing (equal). **Nilanjan Chakraborty:** Conceptualization (equal); Formal analysis (equal); Funding acquisition (lead); Supervision (equal); Writing – original draft (equal).

DATA AVAILABILITY

The data that support the findings of this study are available from the corresponding author upon reasonable request.

REFERENCES

[1] U. Ahmed, N. Chakraborty, and M. Klein, "On the stress-strain alignment in premixed turbulent flames," Sci. Rep. **9**, 5092 (2019).

[2] M. Klein, C. Kasten, Y. Gao, and N. Chakraborty, "A-priori direct numerical simulation assessment of sub-grid scale stress tensor closures for turbulent premixed combustion," Comput. Fluids **122**, 1–11 (2015).

[3] M. Klein, T. Trummler, N. Urban, and N. Chakraborty, "Multiscale analysis of anisotropy of Reynolds stresses, subgrid stresses and dissipation in statistically planar turbulent premixed flames," Appl. Sci. **12**, 2275 (2022).

[4] N. Chakraborty, "Influence of thermal expansion on fluid dynamics of turbulent premixed combustion and its modelling implications," Flow. Turbul. Combust. **106**, 753–806 (2021).

[5] R. A. Antonia, L. Djenidi, and P. R. Spalart, "Anisotropy of the dissipation tensor in a turbulent boundary layer," Phys. Fluids **6**, 2475–2479 (1994).

[6] N. Chakraborty, C. Kasten, U. Ahmed, and M. Klein, "Evolutions of strain rate and dissipation rate of kinetic energy in turbulent premixed flames," Phys. Fluids **33**, 125132 (2021).

[7] M. Leschziner, *Statistical Turbulence Modelling for Fluid Dynamics— Demystified*, 1st ed. (Imperial College Press, 2015).

[8] D. Bradley, P. H. Gaskell, and X. J. Gu, "Application of a Reynolds stress, stretched flamelet, mathematical model to computations of turbulent burning velocities and comparison with experiments," Combust. Flame **96**, 221–248 (1994).

[9] P. Bailly, D. Garréton, O. Simonin, P. Bruel, M. Champion, B. Deshaies, S. Duplantier, and S. Sanquer, "Experimental and numerical study of a premixed flame stabilized by a rectangular section cylinder," Symp. (Int.) Combust. **26**, 923–929 (1996).

[10] P. Bailly, M. Champion, and D. Garréton, "Counter-gradient diffusion in a confined turbulent premixed flame," Phys. Fluids **9**, 766–775 (1997).

[11] L. Tian and R. P. Lindstedt, "The impact of dilatation, scrambling, and pressure transport in turbulent premixed flames," Combust. Theory Modell. **21**, 1114–1147 (2017).

[12] R. P. Lindstedt and E. M. Váos, "Modeling of premixed turbulent flames with second moment methods," Combust. Flame **116**, 461–485 (1999).

[13] S. Hogg and M. A. Leschziner, "Second-moment-closure calculation of strongly swirling confined flow with large density gradients," Int. J. Heat Fluid Flow **10**, 16–27 (1989).

[14] S. Hogg and M. A. Leschziner, "Computation of highly swirling confined flow with a Reynolds stress turbulence model," AIAA J. **27**, 57–63 (1989).

[15] K. Hanjalić and B. E. Launder, *Modelling Turbulence in Engineering and the Environment (Second-Moment Routes to Closure)* (Cambridge University Press, 2011).

[16] K. N. Bray, P. A. Libby, and J. B. Moss, "Unified modeling approach for premixed turbulent combustion—Part I," Combust. Flame **61**, 87–102 (1985).

[17] K. N. C. Bray and P. A. Libby, "Passage times and flamelet crossing frequencies in premixed turbulent combustion," Combust. Sci. Technol. **47**, 253–274 (1986).

[18] H. Kolla, J. W. Rogerson, N. Chakraborty, and N. Swaminathan, "Scalar dissipation rate modeling and its validation," Combust. Sci. Technol. **181**, 518–535 (2009).

[19] U. Ahmed, N. Chakraborty, and M. Klein, "Influence of flow configuration and thermal wall boundary conditions on turbulence during premixed flame-wall interaction within low Reynolds number boundary layers," Flow. Turbul. Combust. **111**, 825–866 (2023).

[20] S. K. Ghai, U. Ahmed, M. Klein, and N. Chakraborty, "Turbulent kinetic energy evolution in turbulent boundary layers during head-on interaction of premixed flames with inert walls for different thermal boundary conditions," Proc. Combust. Inst. **39**, 2169–2178 (2023).

[21] N. Chakraborty, M. Katragadda, and R. S. Cant, "Statistics and modelling of turbulent kinetic energy transport in different regimes of premixed combustion," Flow. Turbul. Combust. **87**, 205–235 (2011).

[22] N. Chakraborty, M. Katragadda, and R. S. Cant, "Effects of Lewis number on turbulent kinetic energy transport in premixed flames," Phys. Fluids **23**, 075109 (2011).

[23] A. R. Varma, U. Ahmed, and N. Chakraborty, "Effects of body forces on turbulent kinetic energy transport in premixed flames," Flow. Turbul. Combust. **109**, 143–173 (2022).

[24] H. Iacovides, B. E. Launder, and A. West, "A comparison and assessment of approaches for modelling flow over in-line tube banks," Int. J. Heat Fluid Flow **49**, 69–79 (2014).

19 April 2024 12:11:51

[25]J. L. Lumley and G. R. Newman, "The return to isotropy of homogeneous turbulence," J. Fluid Mech. **82**, 161–178 (1977).

[26]S. Nishiki, T. Hasegawa, R. Borghi, and R. Himeno, "Modeling of flame-generated turbulence based on direct numerical simulation databases," Proc. Combust. Inst. **29**, 2017–2022 (2002).

[27]D. C. Wilcox, *Turbulence Modeling for CFD*, 3rd ed. (DCW Industries, Inc, 2006).

[28]K. Hanjalić and B. E. Launder, "Contribution towards a Reynolds-stress closure for low-Reynolds-number turbulence," J. Fluid Mech. **74**, 593–610 (1976).

[29]N. N. Mansour, J. Kim, and P. Moin, "Reynolds-stress and dissipation-rate budgets in a turbulent channel flow," J. Fluid Mech. **194**, 15–44 (1988).

[30]B. E. Launder and D. P. Tselepidakis, "Contribution to the modelling of near-wall turbulence," in *Turbulent Shear Flows 8*, edited by F. Durst, R. Friedrich, B. E. Launder, F. W. Schmidt, U. Schumann, and J. H. Whitelaw (Springer, Berlin, Heidelberg, 1993), pp. 81–96.

[31]M. Hallbäck, J. Groth, and A. V. Johansson, "An algebraic model for nonisotropic turbulent dissipation rate in Reynolds stress closures," Phys. Fluids A **2**, 1859–1866 (1990).

[32]K. W. Jenkins and R. S. Cant, "Direct numerical simulation of turbulent flame kernels," in *Recent Advances in DNS and LES*, edited by D. Knight and L. Sakell (Springer, Netherlands, Dordrecht, 1999), pp. 191–202.

[33]U. Ahmed, N. A. K. Doan, J. Lai, M. Klein, N. Chakraborty, and N. Swaminathan, "Multiscale analysis of head-on quenching premixed turbulent flames," Phys. Fluids **30**, 105102 (2018).

[34]J. Lai, M. Klein, and N. Chakraborty, "Direct numerical simulation of head-on quenching of statistically planar turbulent premixed methane-air flames using a detailed chemical mechanism," Flow. Turbul. Combust. **101**, 1073–1091 (2018).

[35]S. K. Ghai, U. Ahmed, and N. Chakraborty, "Effects of fuel Lewis number on wall heat transfer during oblique flame-wall interaction of premixed flames within turbulent boundary layers," Flow. Turbul. Combust. **111**, 867–895 (2023).

[36]U. Ahmed, N. Chakraborty, and M. Klein, "Assessment of Bray Moss Libby formulation for premixed flame-wall interaction within turbulent boundary layers: Influence of flow configuration," Combust. Flame **233**, 111575 (2021).

[37]R. D. Moser, J. Kim, and N. N. Mansour, "Direct numerical simulation of turbulent channel flow up to $Re_\tau = 590$," Phys. Fluids **11**, 943–945 (1999).

[38]T. Tsukahara, Y. Seki, H. Kawamura, and D. Tochio, "DNS of turbulent channel flow at very low Reynolds numbers," in *Fourth International Symposium on Turbulence and Shear Flow Phenomena, Williamsburg, VA, USA, 27–29 June* (Begell House Inc., 2005), pp. 935–940.

[39]U. Ahmed, N. Chakraborty, and M. Klein, "Influence of thermal wall boundary condition on scalar statistics during flame-wall interaction of premixed combustion in turbulent boundary layers," Int. J. Heat Fluid Flow **92**, 108881 (2021).

[40]F. Zentgraf, P. Johe, A. Nicolas, R. S. Barlow, B. Böhm, B. Peterson, and A. Dreizler, "On the evolution of turbulent boundary layers during flame–wall interaction investigated by highly resolved laser diagnostics," Combust. Flame **261**, 113276 (2024).

[41]T. M. Alshaalan and C. J. Rutland, "Wall heat flux in turbulent premixed reacting flow," Combust. Sci. Technol. **174**, 135–165 (2002).

[42]T. M. Alshaalan and C. J. Rutland, "Turbulence, scalar transport, and reaction rates in flame-wall interaction," Symp. (Int.) Combust. **27**, 793–799 (1998).

[43]A. Gruber, R. Sankaran, E. R. Hawkes, and J. H. Chen, "Turbulent flame-wall interaction: A direct numerical simulation study," J. Fluid Mech. **658**, 5–32 (2010).

[44]M. Rißmann, C. Jainski, M. Mann, and A. Dreizler, "Flame-flow interaction in premixed turbulent flames during transient head-on quenching," Flow. Turbul. Combust. **98**, 1025–1038 (2017).

[45]C. Jainski, M. Rißmann, B. Böhm, and A. Dreizler, "Experimental investigation of flame surface density and mean reaction rate during flame-wall interaction," Proc. Combust. Inst. **36**, 1827–1834 (2017).

[46]D. Veynante, A. Trouvé, K. N. Bray, and T. Mantel, "Gradient and counter-gradient scalar transport in turbulent premixed flames," J. Fluid Mech. **332**, 263–293 (1997).

[47]P. A. Durbin and C. G. Speziale, "Local anisotropy in strained turbulence at high Reynolds numbers," J. Fluids Eng. **113**, 707–709 (1991).

[48]J. L. Lumley, "Introduction to 'prediction methods for turbulent flow'," Lecture Series at Von Karman Institute, Belgium, 1975.

19 April 2024 12:11:51